Physical Properties of ZnO-NPs Induced by the Thermal Annealing of Hydrozincite Derived from *Adansonia Digitata* Leaves Extract

I. Ngom[1,2,3]
https://orcid.org/0000-0002-8107-6546
idngom@yahoo.fr

A. Fall[1,2,3]
https://orcid.org/0000-0003-4152-9544

S. Sarr[1]
https://orcid.org/0000-0002-3584-5578

B. M. Ndiaye[1]
https://orcid.org/0009-0008-1053-1549

S. Mbodj[1]
https://orcid.org/0009-0005-3831-1343

R. Bucher[2]
https://orcid.org/0000-0002-0114-6939

B. D. Ngom[1]
https://orcid.org/0000-0003-2113-6057

Abstract

In this study, we investigated the effects of the annealing temperatures on the physical properties of zinc oxide nanoparticles produced by the decomposition of the hydrozincite obtained from *Adansonia digitata* leaves. The results of the X-ray diffraction revealed the formation of well-crystallised hexagonal zinc oxide with an average crystallite size of 11.80 nm, 11.90 nm, 11.97 nm and 15.28 nm for the samples annealed at 400 °C, 500 °C, 600 °C and 700 °C, respectively. The crystallite size of the hydrozincite constituting the unannealed sample was 22 nm. In the spectra of the Fourier transform infrared spectroscopy, the appearance of the peaks at 520 cm^{-1} for all synthesised materials confirms the formation of pure wurtzite zinc oxide. The band gap determined from diffuse reflectance ultraviolet-visible spectroscopy was found to be 3.19 eV, 3.21 eV, 3.23 eV and 3.24 eV for the samples annealed at 400 °C, 500 °C, 600 °C and 700 °C, respectively. These values increase with the annealing temperature and are still lower than the band gap of pure bulk zinc oxide (3.3 eV) owing to the structural defects as confirmed by the broad emission bands in the visible depicted from the photoluminescence analysis.

Keywords: *Adansonia digitata*; ZnO-NPs; annealing temperatures; structural properties; optical properties

1 Quantum Photonics, Energies and Nanofabrication Laboratory, Faculty of Science and Technology, Cheikh Anta Diop University of Dakar, Senegal.
2 Nanosciences Africa Network, iThemba LABS–National Research Foundation, South Africa.
3 UNESCO–UNISA Africa Chair in Nanoscience and Nanotechnology, College of Graduate Studies, University of South Africa.

UNISA university of south africa PRESS
Nano-Horizons
Volume 2 | 2023 | 15 pages

Nano-Horizons
https://doi.org/10.25159/3005-2602/13789
ISSN 3005-2602 (Online)

1 Introduction

In the last ten years, the production of metal oxide nanoparticles from plant extracts has attracted the interest of many researchers [1]. Transitional metal oxide nanoparticles were successfully synthesised via this green and eco-friendly approach such as zinc oxide (ZnO) [2], zirconium oxide (ZrO_2) [3], cadmium oxide (CdO) [4], titanium oxide (TiO_2) [5], nickel oxide (NiO) [6] and copper oxide (CuO) [7]. Owing to its physicochemical properties including non-toxicity, high transparency, good stability, broad direct band gap of 3.3 eV, and high excitonic binding energy of 60 meV at room temperature, ZnO is one of the most studied among them [8]–[11]. All these interesting properties allow the use of ZnO in different domains namely photonics, optoelectronics, medicine and catalysis [10], [12]–[14].

However, during the synthesis process, intermediate complexes can be created at low temperatures before the final metal oxide nanoparticles are obtained at high temperatures. For example, the formation of α-$Ni(OH)_2$ before NiO is reported [15], likewise $Zn_5(CO_3)_2(OH)_6$ before ZnO [16]. The $Zn_5(CO_3)_2(OH)_6$ complex known as hydrozincite belongs to the space group C2/m in the monoclinic phase with lattice parameters a = 13.62 Å, b = 6.300 Å, c = 5.420 Å, and β = 95.50° [17]. In this structure, the Zn atoms are involved in octahedral coordination and tetrahedral coordination at a proportion of 3:2. A successful synthesis of this mineral in the laboratory via different techniques including biosynthesis [18], sol-gel [19], hydrothermal [20] was demonstrated. Hales and Frost [21] reported the hydrothermal synthesis and thermal stability of hydrozincite and smithsonite, two synthetic minerals of zinc. Their results indicated that the zinc carbonate mineral (hydrozincite) is thermally more stable than the zinc hydroxyl-carbonate mineral (smithsonite). Also, Dieng *et al.* [16] reported the biosynthesis of ZnO-NPs via the thermal decomposition of hydrozincite obtained from peanut shell extract. The ZnO-NPs formed after annealing at 500 °C for 4 h were well crystallised with 31.11 nm as the average grain size. Similarly, Kane *et al.* [18] reported the physical properties of ZnO-NPs synthesised from natural extracts of *Adansonia digitata* leaves. Before the thermal treatment, the brown dried sample which was mainly formed of hydrozincite led to the formation of ZnO-NPs after the annealing for 3 h at 500 °C. Equation (1) gives the process governing the heat decomposition of hydrozincite, leading to the formation of zinc oxide.

$$Zn_5(CO_3)_2(\mathrm{OH})_6 \xrightarrow{\Delta} 5\mathrm{ZnO} + 2CO_2 + 3H_2O \quad (1)$$

However, the proper control of the size of nanoparticles and their band gap remains a challenge because the applications of nanoparticles depend on their structural and optical properties. These important properties are directly affected by the synthesis methods and the experimental conditions, in particular, the annealing temperature which occupies a central part.

In this study, we aim to investigate the structural and optical properties of ZnO-NPs produced at different annealing temperatures of hydrozincite obtained from *Adansonia digitata* leaves extract.

Adansonia digitata, also known as baobab, is a member of the *Malvaceae* family. It is a long-lived (over 1 000 years) and big tree native to Africa and grows in arid and semi-arid areas [22], [23]. It has multipurpose uses in daily life owing to the composition of its different parts. For instance, all the parts of *Adansonia digitata*, namely the leaves, flowers, seeds, roots, and fruit pulp, are useful in medicine as an antioxidant, antipyretic, antidiarrheal, and anti-dysentery [24]. The *Adansonia digitata* leaf and stem bark extracts in both alcohol and water had excellent antibacterial activity [2]. Also, in the nutritional domain, *Adansonia digitata* leaves and the fruit's pulp are used to prepare certain sauces and juices. The ability of organic compounds found in plants to act as capping and/or oxidation or reduction agents for the synthesis of nanoparticles has also been proven. These bioactive substances can simply be isolated from diverse parts of the plants. *Adansonia digitata* leaf extract contains many phytochemicals including fatty acids (palmitic acid, oleic acid, linoleic acid), phenols, saponins, alkaloids, flavonoids, tannins, cardiac glucosides, proteins, steroids, terpenoids, vitamins and free amino acids [25]–[27]. All of these molecules, in particular the fatty acids and the phenolic compounds, are both powerful reducers and stabilisers in biosynthesis owing to their carbonyl and hydroxyl groups [28]. In addition, minerals such as sodium (Na), magnesium (Mg), calcium (Ca), potassium (K), iron (Fe), zinc (Zn), copper (Cu), and manganese (Mn) are contained in the leaves of *Adansonia digitata* [29].

Through a variety of characterisation techniques, including X-ray diffraction (XRD), Fourier transform infrared spectroscopy (FTIR), UV-Visible-NIR in diffuse reflectance, and room temperature photoluminescence (PL), we examined the effects of the annealing temperatures (400 °C, 500 °C, 600 °C, and 700 °C) on ZnO-NPs physical properties.

2 Materials and Methods

2.1 Preparation of the Extract

The *Adansonia digitata* leaves used in this study were collected at Bambey Serere (Senegal) in October 2019. These leaves were dried under sunlight and reduced manually to small pieces. They were then used without any other physical or chemical treatment. In a typical setup, as shown in Fig. 1, 9.0 g of these dried leaves were mixed with 300 ml of deionised water contained in a beaker. This mixture, well covered with a white paper towel, was kept at atmospheric conditions for 24 h and then filtered using a paper filter (LTFP-1-090) to separate any residual solids from the extract. A clear and viscous solution extract was produced.

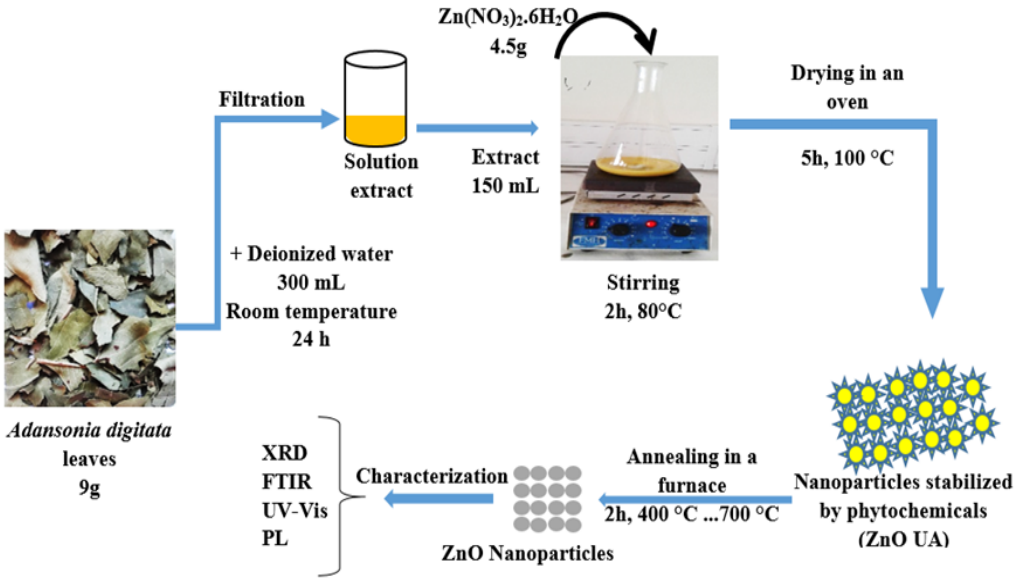

Fig. 1. Schematic diagram of the biosynthesis process of *Adansonia digitata* mediated ZnO nanoparticles.

2.2 Biosynthesis of ZnO Nanoparticles

The precursor used in this synthesis is the zinc nitrate hexahydrate $Zn(NO_3)_2.6H_2O$ (99.99% purity) which was purchased factually from Sigma Aldrich. Because of its high purity, no further purification was needed. For the synthesis, 4.5 g of zinc nitrate hexahydrate was dissolved in 150 ml of the previously extracted solution and the mixture was heated at about 80 °C for 2 h under magnetic stirring. The concentrated solution was then dried in an electric oven at 100 °C for about 5 h which led to the formation of expensed brown solid regarded as the unannealed sample. Four parts of this obtained product were finally annealed in an open furnace for 2 h each at 400 °C, 500 °C, 600 °C, and 700 °C, respectively. White powders were finally formed which constituted the annealed samples.

2.3 Characterisation Techniques

The structural properties of the materials were analysed from a diffractometer (Bruker AXS D8 Advance) using a radiation $\lambda_{CuK\alpha1}$ = 1.54056 Å in 2θ/θ configuration with 0.034° as step size and 2θ values varying from 20° to 80°. The functional groups identified in the annealed and unannealed samples were investigated via a Thermo-Nicolet 8700 Fourier-transform infrared spectrometer. A transparent pellet of each sample mixed with a small amount of potassium bromide (KBr) was made for the analysis. The optical properties of the nanoparticles were depicted firstly using a spectrometer Carry 5000 UV-Vis-NIR operating in the wavelengths from 200 nm to 1 200 nm. A QE Pro High-Performance Spectrometer with an excitation wavelength of 250 nm was then used for the photoluminescence properties.

3 Results and Discussion

3.1 Structural Properties

Fig. 2 reports the XRD spectrum of the as-prepared sample from *Adansonia digitata* leaves extract before annealing. This unannealed sample exhibits a polycrystalline phase with characteristic diffraction peaks attributed to the monoclinic phase of zinc hydroxide carbonate known as hydrozincite $Zn_5(CO_3)_2(OH)_6$ (JCPDS 072-1100 and JCPDS 9007481) [20]. By applying Debye-Scherrer's formula (2) to the most intense peak corresponding to the plan (020), an average crystallite size of 22 nm is found for the hydrozincite nanoparticles.

$$\emptyset = \frac{0.94\lambda}{\Delta COS\theta} \quad (2)$$

Where $\emptyset$ corresponds to the crystallite size (nm), λ = 1.54056 Å is the wavelength of the radiation used, θ represents the Bragg diffraction angle and Δ designates the full width at half maximum of the peak (rad).

For the spectra of annealed samples represented in Fig. 3, all the observed peaks are attributed to the pure wurtzite ZnO in hexagonal structure (JCPDS 00-036-1451). The diffraction peaks observed from the sample annealed at 400 °C appear to be weak with low intensities; thus, an increase in the annealing temperature from 500 °C to 700 °C leads to an improvement in peak intensities and sharpness indicating an enhanced crystallinity of the nanoparticles. As represented in Fig. 4, the crystallite size of the nanoparticles increases slightly with the annealing temperature between 400 °C and 600 °C. It was established that an increase in the annealing temperature favours the coalescence of crystallites to produce larger grains leading to an increase in the crystallite size [30]. The average values of the lattice parameters ⟨a⟩ and ⟨c⟩ were deducted from this relation applicable for hexagonal structure (3):

$$d_{hkl} = \left[\frac{4\left(h^2+k^2+hk\right)}{3a^2} + \frac{l^2}{c^2}\right]^{-\frac{1}{2}} \quad (3)$$

Where d_{hkl} represents the interplanar spacing deducted from Bragg's law while *h*, *k*, and *l* correspond to the Miller index defining the plane.

Fig. 5 shows the evolution of the lattice parameters ⟨a⟩ and ⟨c⟩ as a function of the annealing temperature. From 500 °C, both ⟨a⟩ and ⟨c⟩ increase with the annealing temperature.

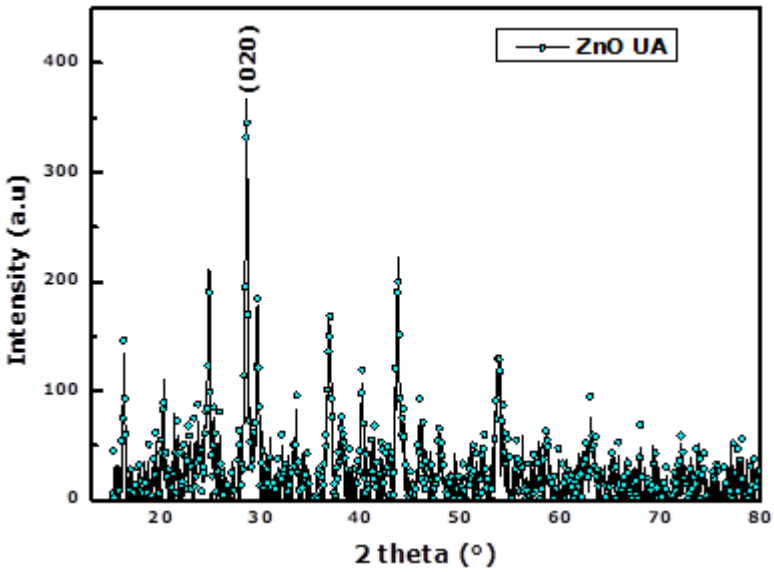

Fig. 2. XRD spectrum of hydrozincite $Zn_5(CO_3)_2(OH)_6$ synthesised from *Adansonia digitata* leaves.

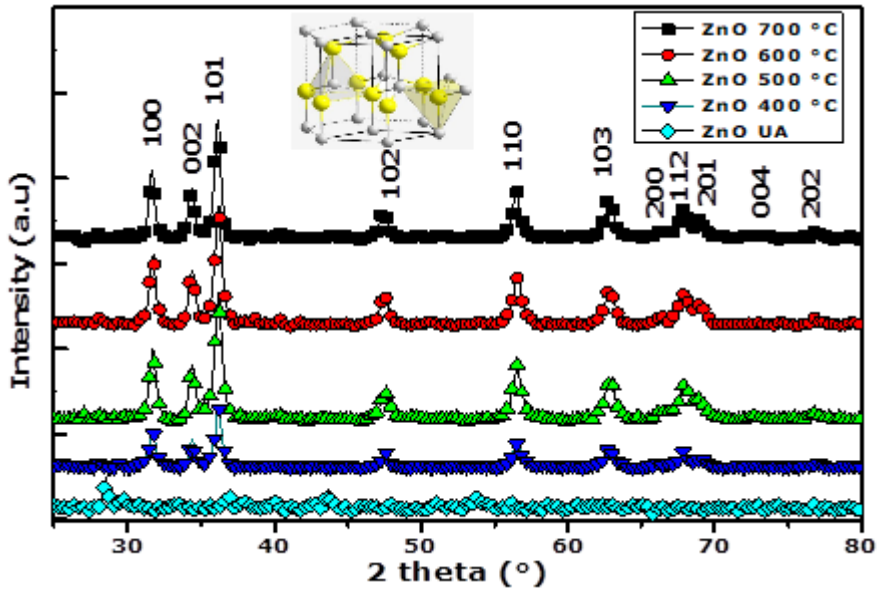

Fig. 3. XRD spectra of ZnO-NPs synthesised from *Adansonia digitata* leaves and annealed at different temperatures.

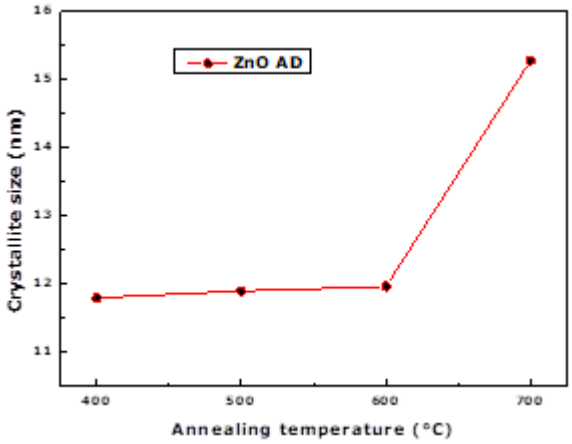

Fig. 4. Evolution of ZnO-NPs crystallite size with annealing temperature.

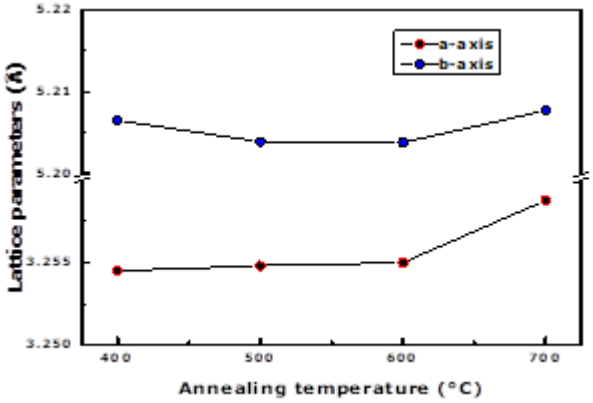

Fig. 5. Evolution of ZnO-NPs lattice parameters with annealing temperature.

To investigate the functional groups of the components present in all the samples, FTIR measurements were conducted in the spectral range of 4 000 cm^{-1}–400 cm^{-1} as presented in Fig. 6. We can observe at high wavenumbers broad bands centred on 3 432 cm^{-1} which are attributed to the asymmetric stretching vibration mode of the O-H bonds [31]. The intensity of this band decreases with the annealing temperature. The peak depicted at 1 640 cm^{-1} corresponds to the symmetric vibration mode of carbonyl bonds C = O [32] of carbonate groups highlighting a possible presence of ester, aldehyde, ketone, or carboxylic acid functions in the unannealed sample. By increasing the annealing temperature, this band is strongly reduced due to the evaporation of the carbon in the form of carbon dioxide as shown previously by equation (1). The intense peaks that appeared at 1 387 cm^{-1} in all spectra are attributed to the symmetric vibrations of the C-O bond originating from *Adansonia digitata* extract.

Furthermore, the peaks observed at 1 056 cm^{-1} could be due to the stretching vibration modes (υ_1) of carbonate groups which denotes the presence of hydrozincite $Zn_5(CO_3)_2(OH)_6$ in the samples [18]. Also, the weak peak that appeared around 820 cm^{-1} in the unannealed sample could be allocated to the (υ_2) bending vibration mode of the carbonate [21]. At low frequencies, in the so-called fingerprint region, we can distinguish the presence of very intense peaks in annealed sample spectra attributed to ZnO, since the vibration modes of the metal-oxygen bonds appear in the range 400 cm^{-1}–600 cm^{-1} [33]. For instance, the peaks appearing around 520 cm^{-1} correspond to the stretching vibration of the Zn-O bond [34], [35]. These FTIR results confirm not only the formation of ZnO-NPs from the thermal decomposition of hydrozincite following the previous XRD results, but also the contribution of bioactive compounds from the plant extract as capping agents.

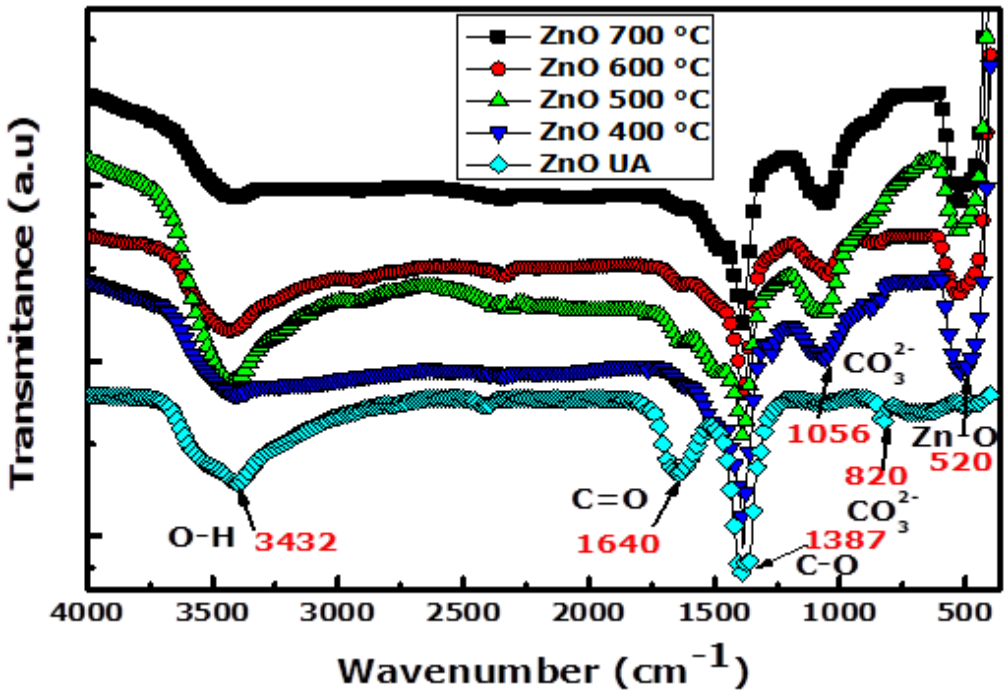

Fig. 6. FTIR spectra of ZnO-NPs synthesised from *Adansonia digitata* leaves and annealed at different temperatures.

3.2 Optical Properties

Diffuse reflectance spectra of the different ZnO samples synthesised with *Adansonia digitata* leaf extracts are shown in Fig. 7. These spectra were recorded in the UV, visible, and near IR regions from 200 nm to 1 200 nm. We note a low reflectance of less than 10 % in the UV domain indicating a strong absorption of $Zn_5(CO_3)_2(OH)_6$ and ZnO nanoparticles. However, from the wavelength 388 nm, the absorption of light by the

ZnO nanoparticles decreases with annealing temperature which justifies the high reflectance up to close 100% in the visible and IR domains. In addition, the band gaps of all the samples were investigated by extrapolating the linear portion of the curve $(\alpha h\upsilon)^2$ against photon energy hυ to the energies axis as shown in Fig. 8(a). Thus, the values of 3.19 eV, 3.21 eV, 3.23 eV, and 3.24 eV were found for the samples annealed at 400 °C, 500 °C, 600 °C, and 700 °C, respectively. These results denote an increase in the band gap with the annealing temperature due to the formation of a more intense phase [36]. These values found are in line with many published studies on the use of plant extracts for the biosynthesis of ZnO nanoparticles [37], [38].

Compared to the most reported bulk band edge value of ZnO (3.3 eV) [11], the low band gap values found for all the annealed samples could be due to the existence of structural defects that create energy levels between the valence band and the conduction band. Likewise, spectroscopic studies on polycrystalline ZnO have shown the presence of an intrinsic energy level at 0.15 eV–0.17 eV below the conduction band [11], [39]. The transition between this donor level and the valence band corresponds to energy below or equal to 3.15 eV which is between 3.1 eV and 3.2 eV as band gap values for bulk ZnO reported by other authors [39]–[41].

Owing to the bioactive compounds from plant extracts covering or changing the surface of the nanoparticles, which causes a blue shift in excitonic absorption [42], the band gap of the unannealed sample (2.44 eV) is less than that of the ZnO-NPs, as shown in Fig. 8(b).

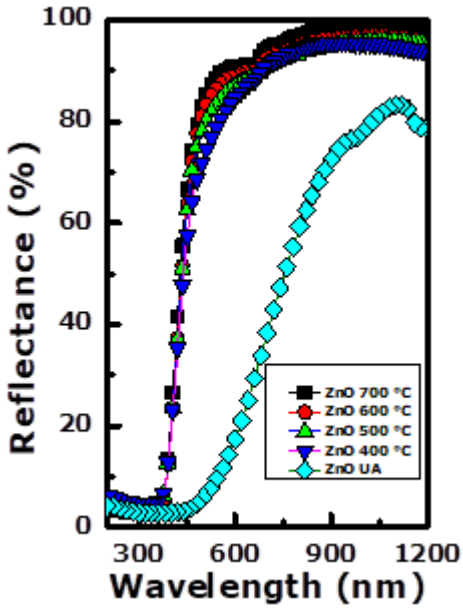

Fig. 7. Diffuse reflectance spectra of ZnO-NPs synthesised from *Adansonia digitata* leaves and annealed at different temperatures.

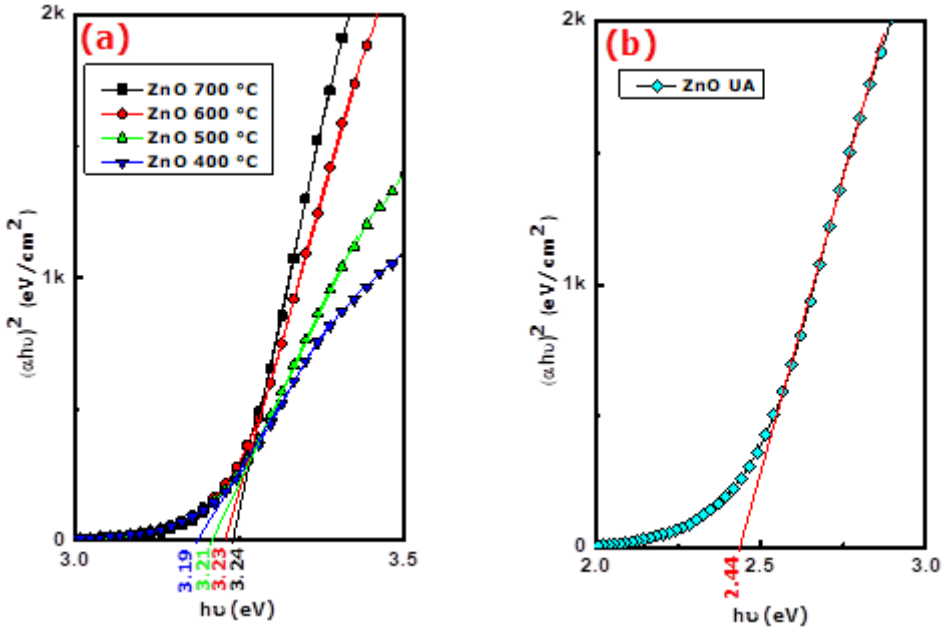

Fig. 8. Band gap calculation of ZnO-NPs synthesised from *Adansonia digitata* leaves for (a) annealed samples at different temperatures, and (b) unannealed sample.

Room temperature photoluminescence experiments were performed on all the samples as a follow-up to the study of diffuse reflectance analysis, to probe the nature of the structural defects and the density of the vacancies for optical properties purposes. All the samples were excited using the same UV wavelength λ_{ext} = 250 nm and the obtained spectra are shown in Fig. 9 in the range of 350 nm–1 200 nm. We can notice a difference between the PL spectrum of the unannealed sample compared to all the annealed materials such as the intensity and the peak position. The PL intensities of all the annealed samples increase with the annealing temperature and are far greater than that of the unannealed one. The luminescence spectra of annealed samples were centred on 500 nm while for the unannealed, the spectrum is centred on 537 nm which corresponds to the energies of 2.48 eV and 2.31 eV, respectively. As reported in many previous studies, the deep visible emission of ZnO is related to the impurities [43] and/or structural defects [44] linked to the oxygen vacancies. This emission in the visible can be indexed to the structural defects due to the absence of impurities in XRD analysis for all annealed samples at different temperatures.

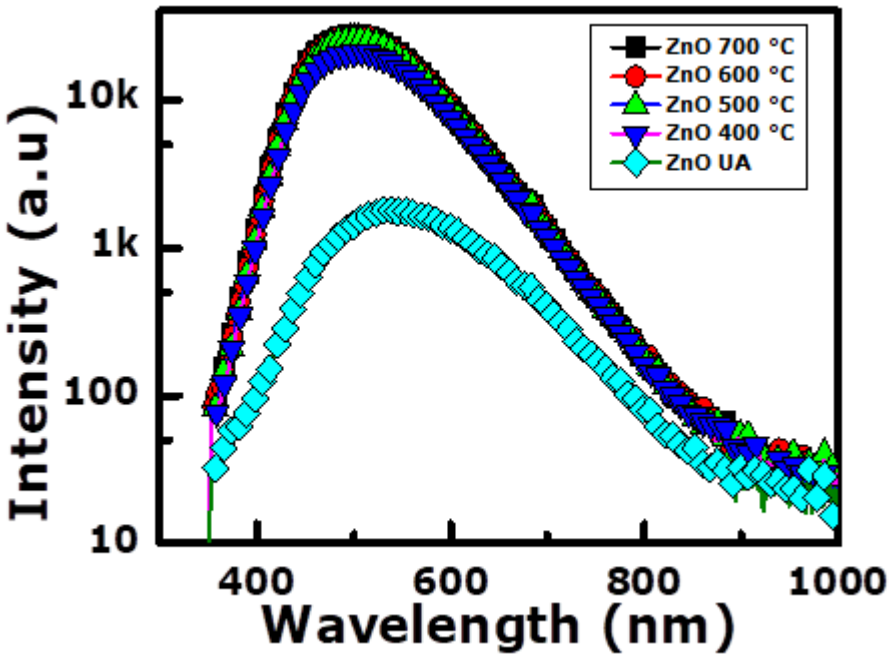

Fig. 9. Room temperature PL spectra of ZnO-NPs synthesised from *Adansonia digitata* leaves and annealed at different temperatures.

4 Conclusion

In this study, we investigated the ways in which the annealing temperatures affected the structural and optical properties of ZnO nanoparticles made by the decomposition of hydrozincite $Zn_5(CO_3)_2(OH)_6$ derived from *Adansonia digitata* leaf extract. The crystallite size of the nanoparticles deducted from XRD analysis and the optical band gap carried out from UV-visible diffuse reflectance studies increase with the annealing temperature which played a significant role in the growth of ZnO-NPs. Using these findings, the annealing temperature can be appropriately adjusted according to the intended application for ZnO nanoparticles. As a follow-up study, we will investigate the reduction mechanism of the zinc precursor by the bioactive compounds present in *Adansonia digitata* leaf extract leading to the formation of hydrozincite.

5 Acknowledgements

We thank the German Academic Exchange Service, the UNESCO-UNISA Africa Chair in Nanosciences and Nanotechnology, the University of South Africa, the Cheikh Anta Diop University of Dakar, and iThemba LABS-National Research Foundation of South Africa for their generous support.

6 References

[1] M. S. Akhtar, J. Panwar, and Y. S. Yun, “Biogenic synthesis of metallic nanoparticles by plant extracts,” *ACS Sustain. Chem. Eng.*, vol. 1, no. 6, pp. 591–602, 2013, doi: 10.1021/sc300118u.

[2] M. Alhujaily *et al.*, “Recent advances in plant-mediated zinc oxide nanoparticles with their significant biomedical properties,” *Bioengineering*, vol. 9, no. 10, p. 541, 2022, doi: 10.3390/bioengineering9100541.

[3] S. Gowri, R. R. Gandhi, and M. Sundrarajan, “Structural, optical, antibacterial and antifungal properties of zirconia nanoparticles by biobased protocol,” *J. Mater. Sci. Technol.*, vol. 30, no. 8, pp. 782–790, 2014, doi: 10.1016/j.jmst.2014.03.002.

[4] N. Thovhogi, E. Park, E. Manikandan, M. Maaza, and A. Gurib-Fakim, “Physical properties of CdO nanoparticles synthesized by green chemistry via Hibiscus Sabdariffa flower extract,” *J. Alloys Compd.*, vol. 655, pp. 314–320, 2016, doi: 10.1016/j.jallcom.2015.09.063.

[5] S. P. Goutam, G. Saxena, V. Singh, A. K. Yadav, R. N. Bharagava, and K. B. Thapa, “Green synthesis of TiO_2 nanoparticles using leaf extract of *Jatropha curcas* L. for photocatalytic degradation of tannery wastewater,” *Chem. Eng. J.*, vol. 336, pp. 386–396, 2018, doi: 10.1016/j.cej.2017.12.029.

[6] I. Ngom, N. M. Ndiaye, N. F. Sylla, S. Dieng, B. D. Ngom, and M. Maaza, “Study of the physical properties of NiO nanoparticles synthesized from the flowers, seeds, and leaves extracts of *Moringa oleifera*, *MRS Adv.*, vol. 8, pp. 729–735, 2023, doi: 10.1557/s43580-023-00578-2.

[7] J. Sackey *et al.*, “Electrochemical properties of *Euphorbia pulcherrima* mediated copper oxide nanoparticles,” *Mater. Chem. Phys.*, vol. 244, p. 122714, 2020, doi: 10.1016/j.matchemphys.2020.122714.

[8] L. Schmidt-Mende, and J. L. MacManus-Driscoll, “ZnO—Nanostructures, defects, and devices,” *Mater. Today*, vol. 10, no. 5, pp. 40–48, 2007, doi: 10.1016/S1369-7021(07)70078-0.

[9] A. Sirelkhatim *et al.*, “Review on zinc oxide nanoparticles: Antibacterial activity and toxicity mechanism,” *Nano-Micro Lett.*, vol. 7, pp. 219–242, 2015, doi: 10.1007/s40820-015-0040-x.

[10] Z. L. Wang, “ZnO nanostructures: Growth, properties and applications,” *J. Phys. Condens. Matter.*, vol. 16, no. 25, pp. 829–858, 2004, doi: 10.1088/0953-8984/16/25/R01.

[11] V. Srikant, and D. R. Clarke, “On the optical band gap of zinc oxide,” *J. Appl. Phys.*, vol. 83, no. 10, pp. 5447–5451, 1998, doi: 10.1063/1.367375.

[12] J. Suresh, G. Pradheesh, V. Alexramani, M. Sundrarajan, and S. I. Hong, "Green synthesis and characterization of zinc oxide nanoparticle using insulin plant (*Costus pictus D. Don*) and investigation of its antimicrobial as well as anticancer activities," *Adv. Nat. Sci. Nanosci. Nanotechnol.*, vol. 9, no. 1, pp. 1–8, 2018, doi: 10.1088/2043-6254/aaa6f1.

[13] S. Karthik, P. Siva, K. S. Balu, R. Suriyaprabha, V. Rajendran, and M. Maaza, "*Acalypha indica*-mediated green synthesis of ZnO nanostructures under differential thermal treatment: Effect on textile coating, hydrophobicity, UV resistance, and antibacterial activity," *Adv. Powder Technol.*, vol. 28, no. 12, pp. 3184–3194, 2017, doi: 10.1016/j.apt.2017.09.033.

[14] E. A. S. Dimapilis, C. Hsu, M. R. O. Mendoza, and M.-C. Lu, "Zinc oxide nanoparticles for water disinfection," *Sustain. Environ. Res.*, vol. 28, no. 2, pp. 47–56, 2017, doi: 10.1016/j.serj.2017.10.001.

[15] A. Diallo *et al.*, "Structural, optical and photocatalytic applications of biosynthesized NiO nanocrystals," *Green Chem. Lett. Rev.*, vol. 11, no. 2, pp. 166–175, 2018, doi: 10.1080/17518253.2018.1447604.

[16] M. T. Dieng, B. D. Ngom, P. D. Tall, and M. Maaza, "Biosynthesis of $Zn_5(CO_3)_2(OH)_6$ from Arachis Hypogaea shell (peanut shell) and its conversion to ZnO nanoparticles," *Am. J. Nanomater.*, vol. 7, pp. 1–9, 2019, doi: 10.12691/AJN-7-1-1.

[17] S. Ghose, "The crystal structure of hydrozincite, $Zn_5(OH)_6(CO_3)_2$," *Acta Cryst.*, vol. 17, pp. 1051–1057, 1964, doi: 10.1107/S0365110X64002651.

[18] A. O. Kane *et al.*, "Biosynthesis of ZnO nanoparticles by *Adansonia Digitata* leaves dye extract: Structural and physical properties," *MRS Adv.*, vol. 3, pp. 2487–2497, 2018, doi: 10.1557/adv.2018.272.

[19] R. Wahab, S. G. Ansari, Y. S. Kim, M. A. Dar, and H. S. Shin, "Synthesis and characterization of hydrozincite and its conversion into zinc oxide nanoparticles," *J. Alloys Compd.*, vol. 461, no. 1–2, pp. 66–71, 2008, doi: 10.1016/j.jallcom.2007.07.029.

[20] M. Y. Nassar, M. M. Moustafa, and M. M. Taha, "Hydrothermal tuning of the morphology and particle size of hydrozincite nanoparticles using different counterions to produce nanosized ZnO as an efficient adsorbent for textile dye removal," *RSC Adv.*, vol. 48, pp. 42180–42195, 2016, doi: 10.1039/C6RA04855B.

[21] M. C. Hales, and R. L. Frost, "Thermal analysis of smithsonite and hydrozincite," *J. Therm. Anal. Calorim.*, vol. 91, pp. 855–860, 2008, doi: 10.1007/s10973-007-8571-0.

[22] A. Patrut *et al.*, "Radiocarbon dating of a very large African baobab," *Tree Physiol.*, vol. 27, no. 11, pp. 1569–1574, 2007, doi: 10.1093/treephys/27.11.1569.

[23] J. Rahul *et al.*, "*Adansonia digitata* L. (baobab): A review of traditional information and taxonomic description," *Asian Pac. J. Trop. Biomed.*, vol. 5, no. 1, pp. 79–84, 2015, doi: 10.1016/S2221-1691(15)30174-X.

[24] F. J. Chadare, *Baobab (*Adansonia digitata *L.) foods from Benin: Composition, processing and quality*. Wageningen, Netherlands: Wageningen University, 2010.

[25] E. N. Uhuo, S. I. Egba, P. C. Nwuke, C. A. Obike, and G. K. Kelechi, "Antioxidative properties of *Adansonia digitata* L. (baobab) leaf extract exert protective effect on doxorubicin-induced cardiac toxicity in Wistar rats," *Clin. Nutr. Open Sci.*, vol. 45, pp. 3–16, 2022, doi: 10.1016/j.nutos.2022.07.004.

[26] D. Yazzie, D. J. Vanderjagt, A. Pastuszyn, A. Okolo, and R. H. Glew, "The amino acid and mineral content of baobab (*Adansonia digitata* L.) leaves," *J. Food Compos. Anal.*, vol. 7, no. 3, pp. 189–193, 1994, doi: 10.1006/jfca.1994.1018.

[27] E. A. Irondi, J. K. Akintunde, S. O. Agboola, A. A. Boligon, and M. L. Athayde, "Blanching influences the phenolics composition, antioxidant activity, and inhibitory effect of *Adansonia digitata* leaves extract on α-amylase, α-glucosidase, and aldose reductase," *Food Sci. Nutr.*, vol. 5, no. 2, pp. 233–242, 2017, doi: 10.1002/fsn3.386.

[28] M. G. Berhe, and Y. T. Gebreslassie, "Biomedical applications of biosynthesized nickel oxide nanoparticles," *Int. J. Nanomedicine.*, vol. 18, pp. 4229–4251, 2023, doi: 10.2147/IJN.S410668.

[29] C. C. Ogbaga, F. A. Nuruddeen, O. O. Alonge, and O. F. Nwagbara, "Phytochemical, elemental and proximate analyses of stored, sun-dried and shade-dried baobab (*Adansonia digitata*) leaves," in *13th Int. Conf. Electron. Comput. ICECCO 2017*, January 2018, pp. 1–5, doi: 10.1109/ICECCO.2017.8333339.

[30] M. M. El-Okr, M. A. Salem, M. S. Salim, R. M. El-Okr, M. Ashoush, and H. M. Talaat, "Synthesis of cobalt ferrite nano-particles and their magnetic characterization," *J. Magn. Magn. Mater.*, vol. 323, no. 7, pp. 920–926, 2011, doi: 10.1016/j.jmmm.2010.11.069.

[31] P. K. Raul *et al.*, "CuO nanorods: A potential and efficient adsorbent in water purification," *RSC Adv.*, vol. 76, pp. 40580–40587, 2014, doi: 10.1039/C4RA04619F.

[32] Y. Yulizar, R. Bakri, D. Oky, B. Apriandanu, and T. Hidayat, "Nano-structures & nano-objects ZnO/CuO nanocomposite prepared in one-pot green synthesis using seed bark extract of *Theobroma cacao*," *Nano-Structures & Nano-Objects.*, vol. 16, pp. 300–305, 2018, doi: 10.1016/j.nanoso.2018.09.003.

[33] T. V. Surendra, S. M. Roopan, N. A. Al-Dhabi, M. V. Arasu, G. Sarkar, and K. Suthindhiran, "Vegetable peel waste for the production of ZnO nanoparticles and its toxicological efficiency, antifungal, hemolytic, and antibacterial activities," *Nanoscale Res. Lett.*, vol. 11, pp. 1–10, 2016, doi: 10.1186/s11671-016-1750-9.

[34] Y. Gutha, J. L. Pathak, W. Zhang, Y. Zhang, and X. Jiao, "Antibacterial and wound healing properties of chitosan/poly(vinyl alcohol)/zinc oxide beads (CS/PVA/ZnO)," *Int. J. Biol. Macromol.*, vol. 103, pp. 234–241, 2017 doi:10.1016/j.ijbiomac.2017.05.020.

[35] R. Dobrucka, and J. Długaszewska, “Biosynthesis and antibacterial activity of ZnO nanoparticles using *Trifolium pratense* flower extract,” *Saudi J. Biol. Sci.*, vol. 23, no. 4, pp. 517–523, 2016, doi: 10.1016/j.sjbs.2015.05.016.

[36] N. Bala *et al.*, “Green synthesis of zinc oxide nanoparticles using *Hibiscus subdariffa* leaf extract: Effect of temperature on synthesis, anti-bacterial activity and anti-diabetic activity,” *RSC Adv.*, vol. 7, pp. 4993–5003, 2015, doi: 10.1039/C4RA12784F.

[37] N. Matinise, X. G. Fuku, K. Kaviyarasu, N. Mayedwa, and M. Maaza, “ZnO nanoparticles via Moringa *oleifera* green synthesis: Physical properties and mechanism of formation,” *Appl. Surf. Sci.*, vol. 406, pp. 339–347, 2017, doi: 10.1016/j.apsusc.2017.01.219.

[38] A. T. Khalil *et al.*, “*Sageretia thea* (Osbeck.) mediated synthesis of zinc oxide nanoparticles and its biological applications,” *Nanomedicine.*, vol. 12, no. 15, pp. 1767–1789, 2017, doi: 10.2217/nnm-2017-0124.

[39] F. Greuter, and G. Blatter, “Electrical properties of grain boundaries in polycrystalline compound semiconductors,” *Semicond. Sci. Technol.*, vol. 5, no. 2, pp. 111–137, 1990, doi: 10.1088/0268-1242/5/2/001.

[40] J. Kossanyi *et al.*, “Photoluminescence of semiconducting zinc oxide containing rare earth ions as impurities,” *J. Lumin.*, vol. 46, no. 1, pp. 17–24, 1990, doi: 10.1016/0022-2313(90)90077-O.

[41] M. Liu, A. H. Kitai, and P. Mascher, “Point defects and luminescence centres in zinc oxide and zinc oxide doped with manganese,” *J. Lumin.*, vol. 54, no. 1, pp. 35–42, 1992, doi: 10.1016/0022-2313(92)90047-D.

[42] F. N. Alharbi, Z. M. Abaker, and S. Z. A. Makawi, “Phytochemical substances—Mediated synthesis of zinc oxide nanoparticles (ZnO NPS),” *Inorganics*, vol. 11, no. 8, pp. 3281–3294, 2023, doi: 10.3390/inorganics11080328.

[43] J. Lv, and M. Fang, “Photoluminescence study of interstitial oxygen defects in ZnO nanostructures,” *Mater. Lett.*, vol. 218, pp. 18–21, 2018, doi: 10.1016/j.matlet.2018.01.137.

[44] L. Zhang, J. Zhao, J. Zheng, L. Li, and Z. Zhu, “Shuttle-like ZnO nano/microrods: Facile synthesis, optical characterization and high formaldehyde sensing properties,” *Appl. Surf. Sci.*, vol. 258, no. 2, pp. 711–718, 2011, doi: 10.1016/j.apsusc.2011.07.116.